Supplemental material for: 'Finding a junction partner for candidate solar cell absorbers enargite and bournonite from electronic band and lattice matching'

Suzanne K. Wallace[a,b], Keith T. Butler[c], Yoyo Hinuma[d,e], and Aron Walsh*[b,f]

[a] ***Department of Chemistry, Centre for Sustainable Chemical Technologies, University of Bath, Claverton Down, Bath, BA2 7AY, UK***

[b] ***Department of Materials, Imperial College London, Exhibition Road, London SW7 2AZ, UK. Email: a.walsh@imperial.ac.uk***

[c] ***ISIS Neutron and Muon Source, Rutherford Appleton Laboratories, Didcot, Oxfordshire, OX11 0QX***

[d] ***Center for Frontier Science, Chiba University, Chiba 263-8522, Japan***

[e] ***Center for Materials Research by Information Integration, Research and Services Division of Materials Data and Integrated System, National Institute for Materials Science, Tsukuba 305-0047, Japan***

[f] ***Department of Materials Science and Engineering, Yonsei University, Seoul 03722, Korea***

1 Slab models

Symmetric and non-polar surface terminations for enargite (Cu_3AsS_4) and bournonite ($CuPbSbS_3$) cut using methodology in Ref. [2]. The VESTA[4] software package was used to create Fig. 1 and 2.

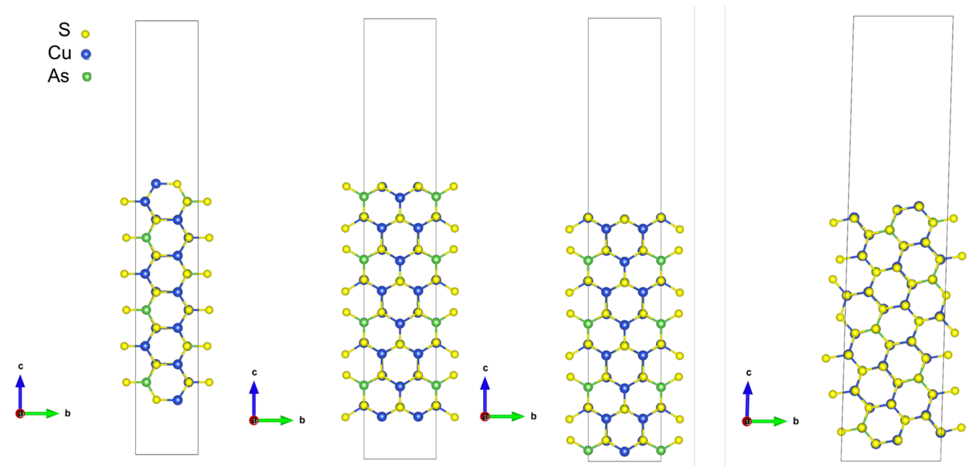

Figure 1: Enargite (Cu_3AsS_4) (100), (010)a, (010)b, (110) surface terminations.

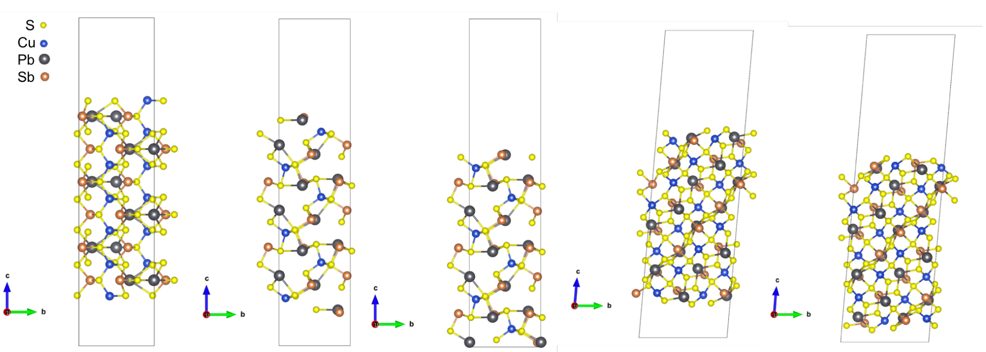

Figure 2: Bournonite ($CuPbSbS_3$) (100), (010)a, (010b), (110)a, (110)b surface terminations.

2 Slab potentials

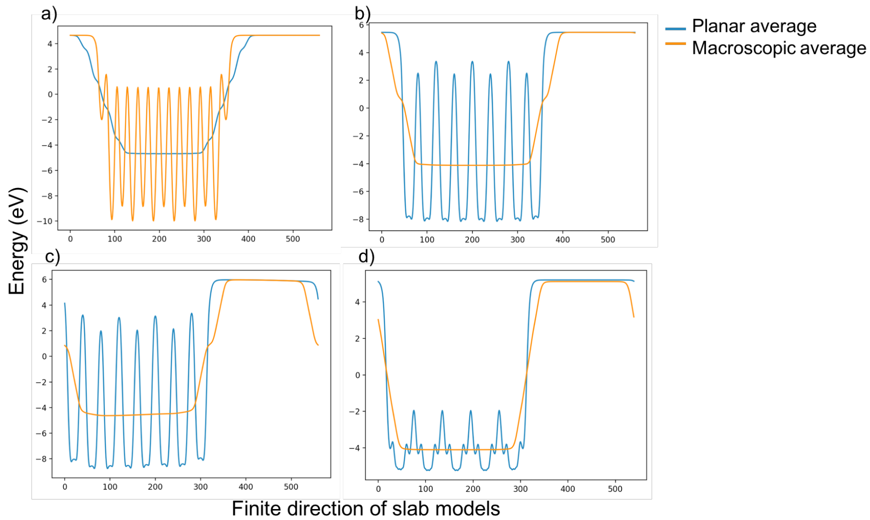

Figure 3: Electrostatic potentials across the finite direction of slab models for enargite (Cu_3AsS_4) a) (100), b) (010)a, c) (010)b, d) (110) surfaces.

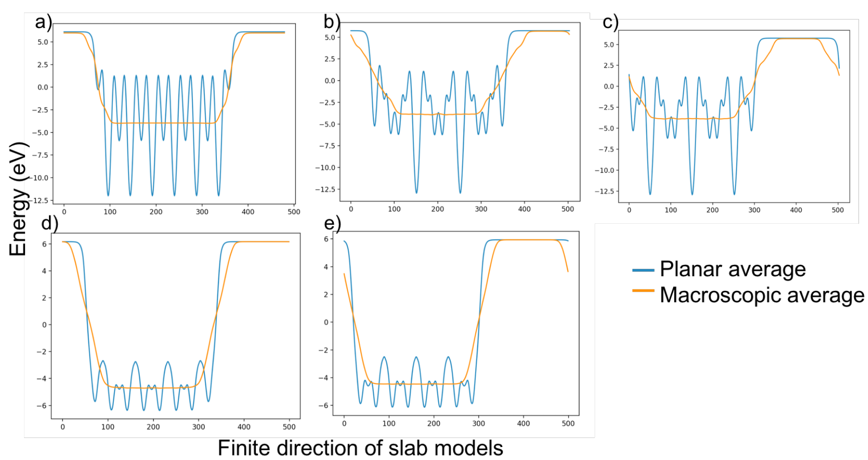

Figure 4: Electrostatic potentials across the finite direction of slab models for bournonite ($CuPbSbS_3$) a) (100), b) (010)a, c) (010)b, d) (110)a, e) (110)b surfaces.

3 Structure files for junction partners used for lattice matching

Table 1: Materials project IDs for structure files used for lattice matching step.

Candidate	Materials project ID
Dy_2S_3	mp-32826
La_2S_3	mp-7475
Nd_2S_3	mp-32586
Sm_2S_3	mp-32645
Tb_2S_3	mp-673644
WO_3	mp-19033
ZnTe	mp-2176
Ce_2S_3	mp-20973
$Zn_3In_2S_6$	mp-637614
SiC	mp-11714
GaP	mp-2490
ZnSe	mp-1190
Ce_2O_3	mp-542313
Bi_2O_3	mp-23262
$CoTiO_3$	mp-19424
$NiTiO_3$	mp-556251
SnS_2	mp-1170
Cu_2O	mp-361
Gd_2S_3	mp-608146
AlP	mp-1550
MoO_3	mp-18856
CuI	mp-570136
As_2S_3	mp-641
CdS	mp-672
PbO	mp-19921
CoO	mp-24864

4 Band alignment with final junction partners candidates for all absorber slabs

Below are band alignment plots of the final junction partner candidates for each absorber layer slab. Ionisation potentials, electronic band gaps and electron affinities for the absorber materials are calculated in this work, but those of the candidate junction partners are from the dataset used in Ref. [1] and contained in the ELS git repository. The minimum strain termination for each junction partner candidate were shown in the main manuscript in Tables 2 and 3.

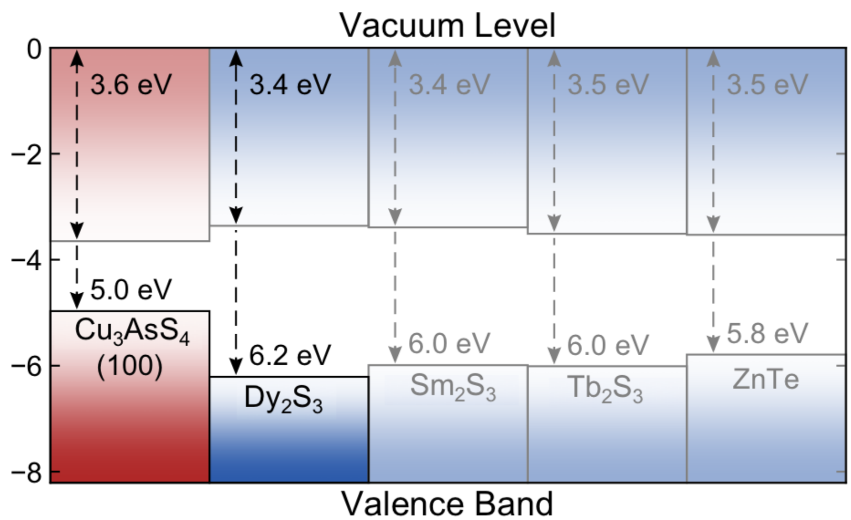

Figure 5: Spike conduction band offset (CBO) for enargite (Cu_3AsS_4) (100) termination.

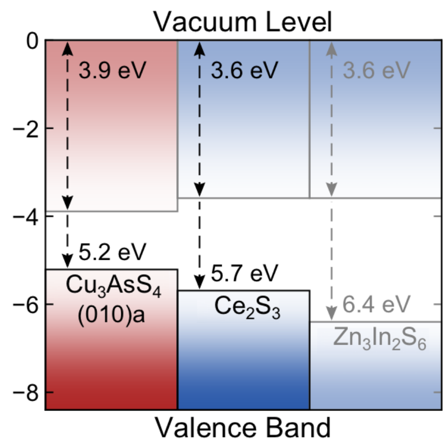

Figure 6: Spike conduction band offset (CBO) for enargite (Cu_3AsS_4) (010)a termination.

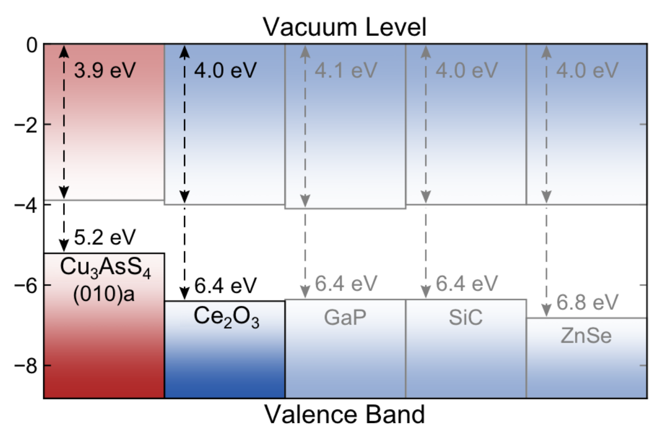

Figure 7: Cliff conduction band offset (CBO) for enargite (Cu_3AsS_4) (010)a termination.

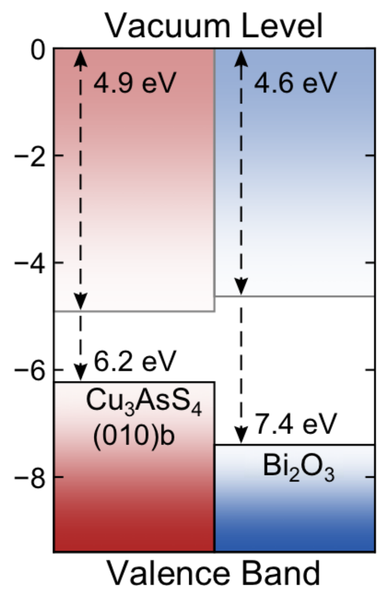

Figure 8: Spike conduction band offset (CBO) for enargite (Cu_3AsS_4) (010)b termination.

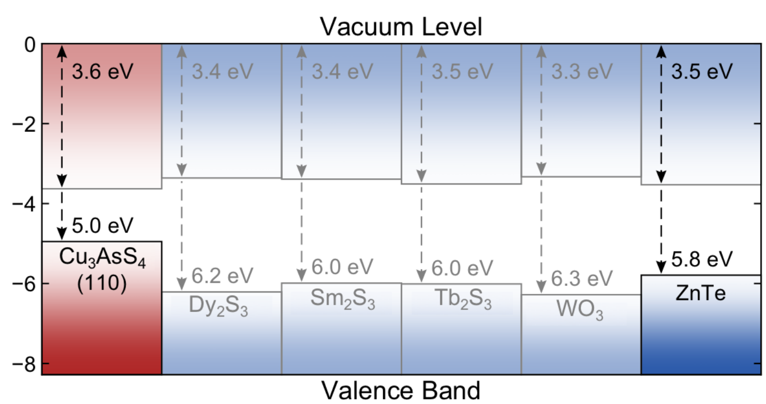

Figure 9: Spike conduction band offset (CBO) for enargite (Cu_3AsS_4) (110) termination.

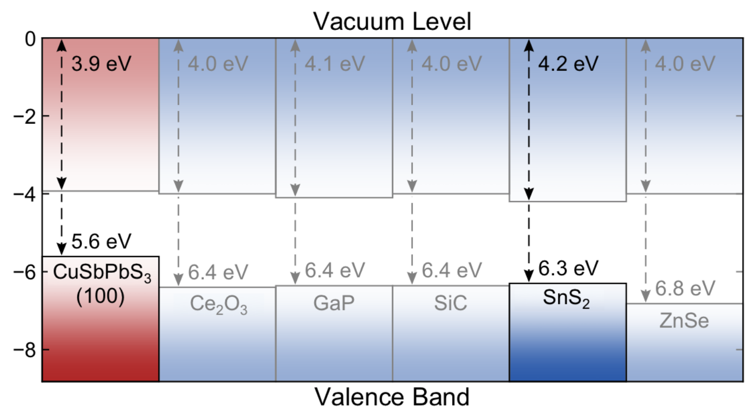

Figure 10: Cliff conduction band offset (CBO) for bournonite ($CuPbSbS_3$) (100) termination.

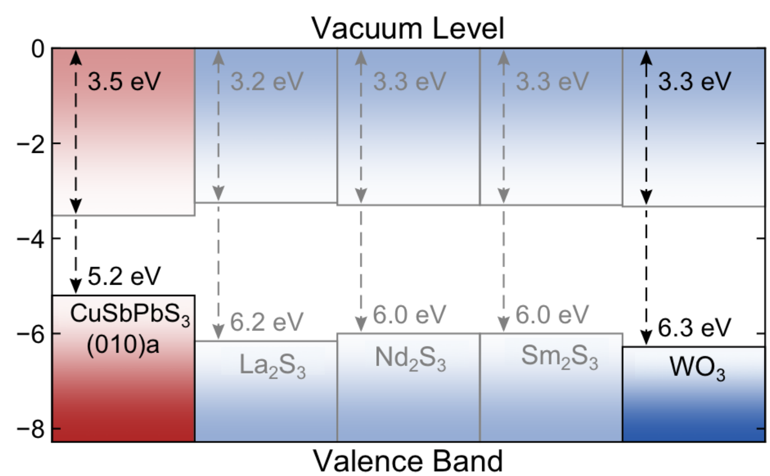

Figure 11: Spike conduction band offset (CBO) for bournonite ($CuPbSbS_3$) (010)a termination.

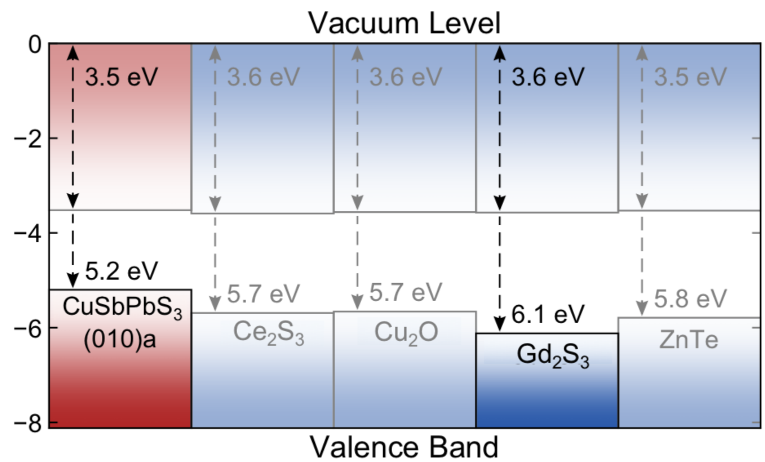

Figure 12: Cliff conduction band offset (CBO) for bournonite ($CuPbSbS_3$) (010)a termination.

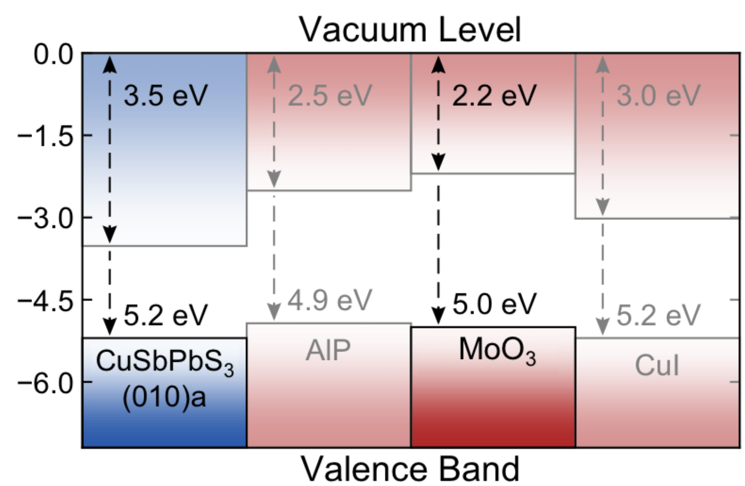

Figure 13: Cliff valence band offset (VBO) for bournonite ($CuPbSbS_3$) (010)a termination.

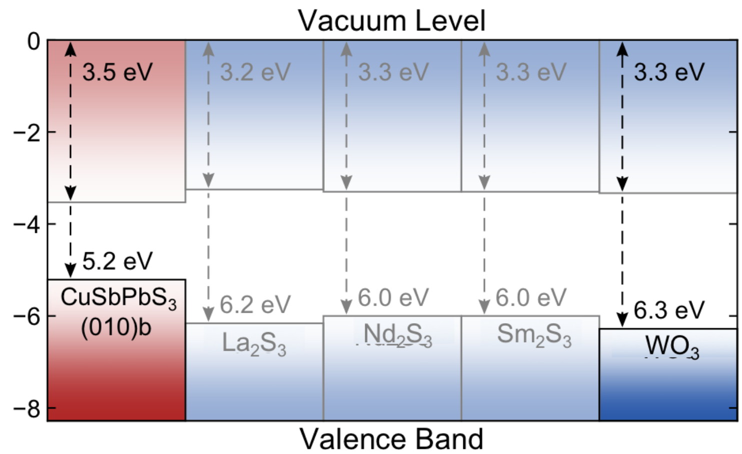

Figure 14: Spike conduction band offset (CBO) for bournonite ($CuPbSbS_3$) (010)b termination.

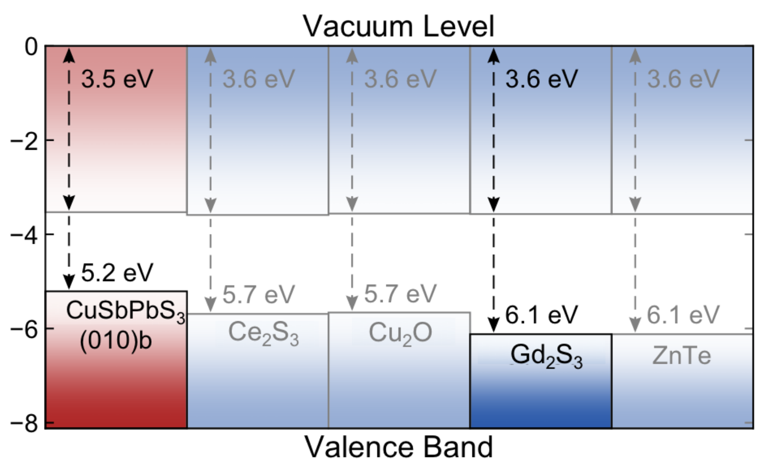

Figure 15: Cliff conduction band offset (CBO) for bournonite ($CuPbSbS_3$) (010)b termination.

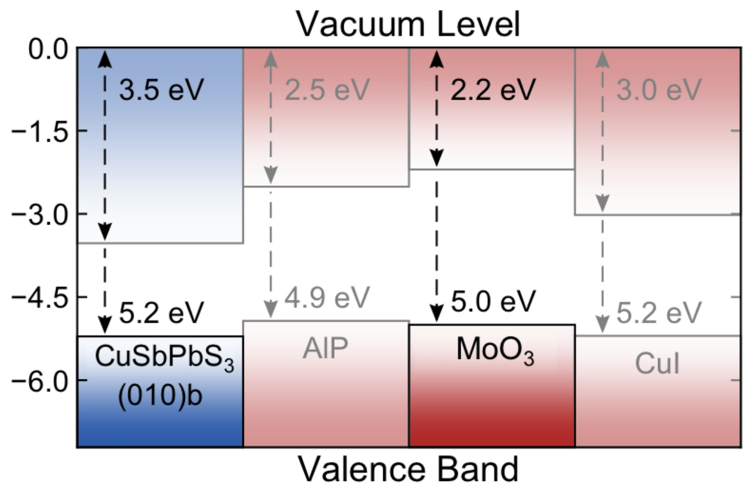

Figure 16: Cliff valence band offset (VBO) for bournonite ($CuPbSbS_3$) (010)b termination.

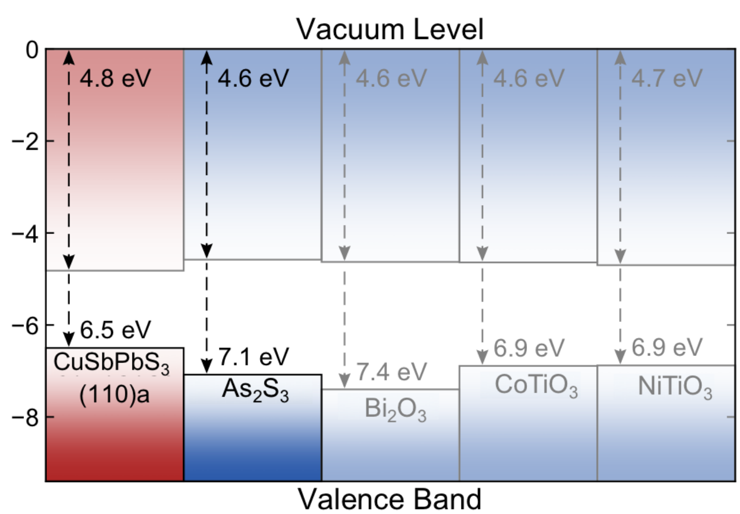

Figure 17: Spike conduction band offset (CBO) for bournonite ($CuPbSbS_3$) (110)a termination.

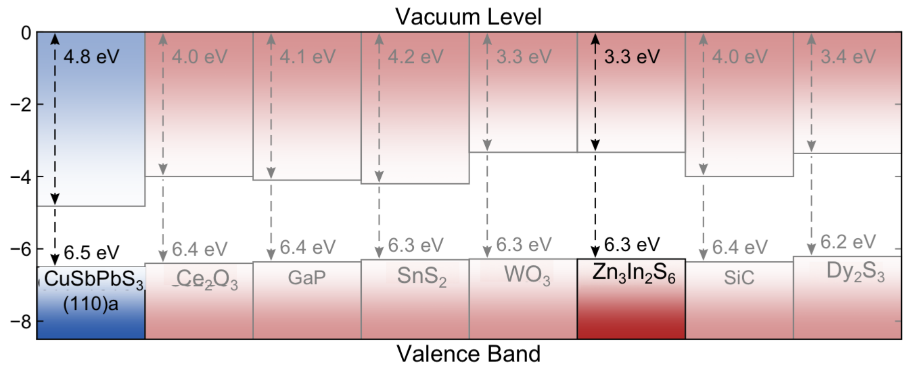

Figure 18: Cliff valence band offset (VBO) for bournonite ($CuPbSbS_3$) (110)a termination.

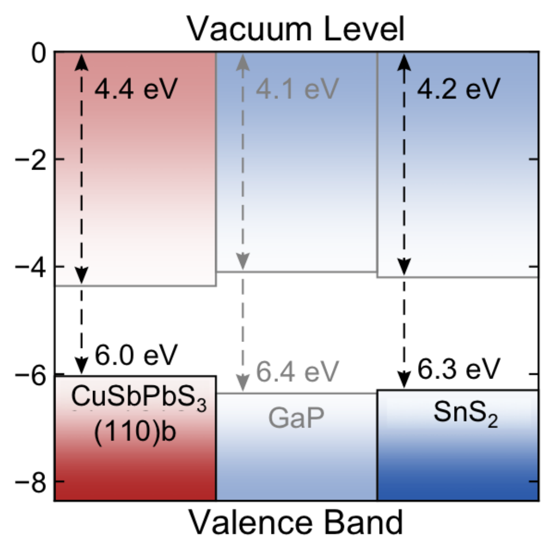

Figure 19: Spike conduction band offset (CBO) for bournonite ($CuPbSbS_3$) (110)b termination.

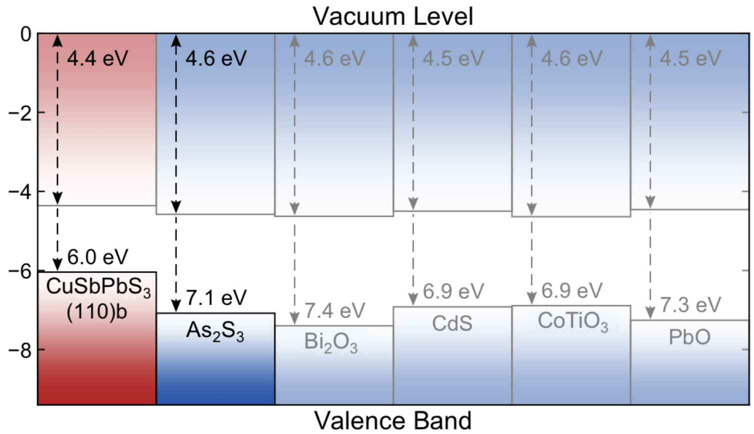

Figure 20: Cliff conduction band offset (CBO) for bournonite ($CuPbSbS_3$) (110)b termination.

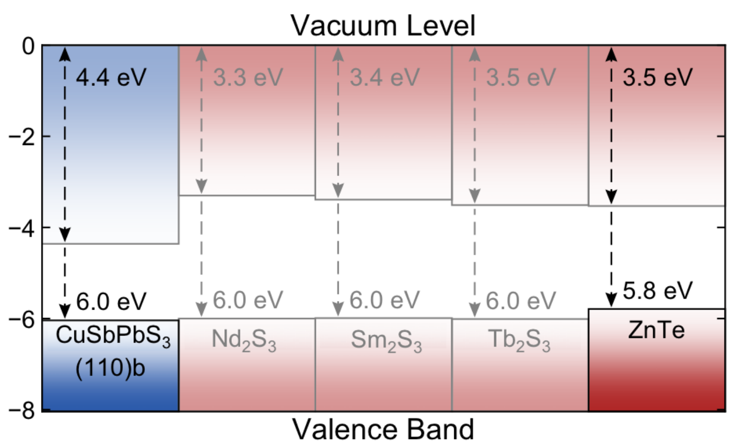

Figure 21: Cliff valence band offset (VBO) for bournonite ($CuPbSbS_3$) (110)b termination.

References

[1] K. T. Butler, Y. Kumagai, F. Oba, and A. Walsh. Screening procedure for structurally and electronically matched contact layers for high-performance solar cells: hybrid perovskites. *J. Mater. Chem. C*, 4(6):1149–1158, 2016.

[2] Y. Hinuma, Y. Kumagai, F. Oba, and I. Tanaka. Categorization of surface polarity from a crystallographic approach. *Computational Materials Science*, 113:221 – 230, 2016.

[3] Y. Kumagai, K. T. Butler, A. Walsh, and F. Oba. Theory of ionization potentials of nonmetallic solids. *Physical Review B*, 95(12), mar 2017.

[4] K. Momma and F. Izumi. VESTA for three-dimensional visualization of crystal, volumetric and morphology data. *Journal of Applied Crystallography*, 44(6):1272–1276, oct 2011.